13 May 1999

Scene Modeling from Motion-Free Radar Sensing

Alex Foessel

Ph.D. Thesis Proposal

Abstract

Sonar, laser and stereo are common sensors used for safeguarding, mapping and navigation in robotic applications. However, vacuum, dust, fog, rain, snow and light conditions found in construction, mining, agricultural and planetary-exploration environments compromise the effectiveness of these sensors. Sonar can not operate in vacuum conditions, low visibility and scanning mechanisms limit laser's reliability, and stereo is dependent on scene texture and illumination.

Radar can offer remarkable advantages as a robotic perception mode because it is not as vulnerable to the aforementioned conditions. Also, radar can be electronically-steered. However, radar has shortcomings such as a large footprint, sidelobes, specularity effects and limited range resolution, all of which result in poor perception models. Some of these problems worsen with the introduction of motion-free scanning, which is important for high reliability and size reduction. Radar's shortcomings provide the context for the proposed research.

I plan to develop an interpreter for building high-resolution and high-fidelity perception models from motion-free scanning radar sensing. Quality maps will make radar an effective tool for numerous robotic applications.

Contents

1.0 Motivation, Problems and Possibilities 3
- 1.1 Motivation 3
- 1.2 Problems 4
- 1.3 Possibilities 4

2.0 Background and Related Work 5
- 2.1 Radar Background 5
- 2.2 Modeling With Short-Range Radar 8
- 2.3 Evidence Grids: a Convenient Representation Tool 10
  - 2.3.1 Representation of Occupancy and Emptiness 10
  - 2.3.2 Evidence Grid Extension: Modeling Surfaces 11

3.0 Technical Approach 12
- 3.1 Radar-Data Heuristics: Identification of Point Targets and Planes 12
- 3.2 Radar-Tailored Evidence Grid with Surface Representation 14
- 3.3 Sidelobe and Reflection Ambiguity Solving from Sensor Motion 15
- 3.4 Sensor Profile: Multilobe Varying Geometry 15
  - 3.4.1 Radar - Multilobe Sensor Profile 16
  - 3.4.2 Evidence from Reflected Beams 16
  - 3.4.3 Variations in the sensor profile 17

4.0 Early Research 18
- 4.1 Radar Experimental Characterization 18
  - 4.1.1 Range-Precision Experiment 19
  - 4.1.2 Range-Resolution Experiment 19
  - 4.1.3 Beamwidth-Estimation Experiment 20
- 4.2 Antenna Performance Variation with Scan Angle 20
- 4.3 Evidence Grid Implementation 21
  - 4.3.1 Single-Target Scene Modeling 21
  - 4.3.2 Concave and Convex Obstacles Modeling 21

5.0 Proposed Research Plan and Schedule 22
- 5.1 Proposed Research 22
- 5.2 Research Tasks 22

6.0 Bibliography 23

A. Radar Properties 25
- A.1 Beamwidth, Frequency and Antenna Aperture 25
- A.2 Range Precision and Resolution 25
- A.3 Specular Surfaces 25
- A.4 Near/Far Field 26

B. Extreme Weather Validation of Radar Sensing 27

1.0 Motivation, Problems and Possibilities

1.1 Motivation

Current research on capable robotic vehicles focuses on the mining, earth-moving and agricultural industries as well as on planetary-exploration applications. Imaging sensors provide obstacle avoidance, task-specific target detection and generation of terrain maps for navigation. Also the sensors provide a means of detecting humans, animals and vehicles entering the workspace.

Visibility conditions are often poor in field-robotic scenarios. Day/night cycles change illumination conditions. Weather phenomena such as fog, rain, snow and hail impede visual perception. Dust clouds rise in excavation sites, agricultural fields and planetary exploration. Also smoke compromises visibility in fire emergencies and battlefield operations.

Laser and stereo are common visually based sensors affected by these conditions. The sizes of dust particles, fog droplets and snow flakes are comparable to the wavelength of visual light so clouds of particles block and disperse the beams impeding perception. Stereo depends on the texture of targets and on an illumination source. Delicate scanning mechanisms limit laser reliability. Current developments in motion-free laser scanning that address this shortcoming are not mature and have limited scanning range.

Sonar is a common sensor not affected by visibility restrictions. However, sonar suffers from reflections by specular surfaces, a limited maximum range, a long settling time and cross coupling. The beamwidth of sonar can be tens of degrees. This results in poor resolution. Software techniques for indoor perception improve the resolution and fidelity of sonar readings with some success. However, results are of limited utility for field robots.

Researchers have explored sensor combinations to overcome the deficiencies of each sensor. Size, complexity and reliability outweigh the convenience of these proposed schemes. Particles still adversely affect visual-sensor combinations.

Millimeter-wave radar provides consistent range measurements for the environmental imaging needed to perform autonomous operations in dusty, foggy, blizzard-blinding and poorly lit environments. Motion-free radar scanning is possible, providing reliable perception over a two-dimensional field-of-view. Radar overcomes the shortcomings of laser, stereo and sonar. However, current developments of short-range radar imaging are not satisfactory.

The generation of short-range perception models from radar is beyond the state of art. High angular resolution can only be obtained with inconveniently large antenna apertures. Mechanical-scanning equipment is heavy and unreliable. Similarly, robot position estimation and navigation based on radar succeed only when relying on artificial landmarks; natural landmarks are hard to distinguish from noise and false targets. Furthermore, the incorporation of motion-free scanning antennas complicates the applicability of radar because the antennas project different beam properties as they scan. Early attempts to build models using short-range radar compare poorly with the perception models built from sonar, laser and stereo sensors.

Current short-range radar perception lacks adequate data-interpretation capabilities. Radar interpretation should account for properties such as sidelobes, reflection, antenna-radiation pattern variation and noise distribution. This presents a research opportunity that could benefit robotics with reliable perception in compromised visibility conditions.

1.2 Problems

Limited range resolution, a large footprint, specular reflection, sidelobe false targets, and changing radiation patterns affect interpretation of radar data. Resulting models can be inaccurate, ambiguous and inconsistent. *Figure 1* illustrates these pitfalls.

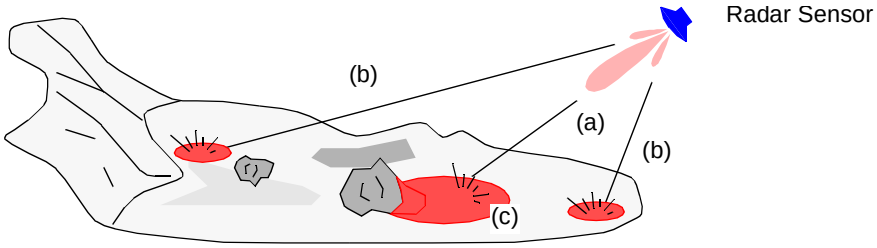

FIGURE 1. A representation of radar interaction with a scene. The emitted energy is concentrated in the mainlobe (a). Some energy leaks through the sidelobes (b), generating returns from other areas of the scene. The mainlobe footprint (c) combines the returns of multiple objects.

Radar-propagation properties adversely affect the resolution and fidelity of perception models. Wide beams have large footprints and combine the returns of multiple targets or large areas. Combination of targets and surfaces results in ambiguous range estimation.

Sidelobes and specular reflections introduce false targets. Sidelobes are low-attenuation zones around the mainlobe that cause the false perception of off-center targets. False targets are also the result of specular effects. Targets reflected by the specular surfaces appear in other locations and the sensor may not perceive the reflecting surface.

The adoption of motion-free techniques to steer a radar beam introduces additional complexities. Traditional antennas provide narrow beams and high rejection of sidelobe false targets, properties that remain constant over the scanning range. The radiation pattern of motion-free scanning antennas changes with each new beam position. The antenna performance degrades at extreme scanning angles: the mainlobe widens, its gain changes and sidelobes have less attenuation.

1.3 Possibilities

Despite radar shortcomings, scene models could be created with vast improvement above what is possible by mapping raw-signal data.

Interpretation of radar data could consider sensor and scene properties, as well as the interaction between them. Radar properties such as output power, range resolution, antenna radiation pattern (beamwidth and sidelobe rejection) and antenna-scanning range might be included. Scene geometry, surface specularity, occlusions and scene change could be represented.

An interpreter could effectively update a scene representation with raw data obtained from a motion-free scanning radar, and increase resolution and fidelity of the resulting perception model.

2.0 Background and Related Work

The technologies of radar propagation, perception representation and sensor-signal interpretation are essential building blocks for an interpreter that will create a scene model from radar data. Discussion of these technologies follows.

2.1 Radar Background

Radar transmits electromagnetic radiation through an antenna [1][2]. As a signal propagates, objects reflect, refract and absorb it. The radiation that returns to the receiving antenna converts to a vector of values representing the received-signal amplitude. Large amplitude provides evidence of a large reflecting object. Low amplitude suggests the absence of any reflecting object. Low amplitude could, however, correspond to a specular reflecting surface or to a highly absorbing material.

Radar cross section represents the ability to return energy to an antenna. It is a function of three parameters: geometric cross section related to the size of the object; reflectivity, that portion of the energy is reflected and not absorbed, and dependent on the material properties; and directivity, a measure of the energy returned to the antenna, which is mainly influenced by target geometry.

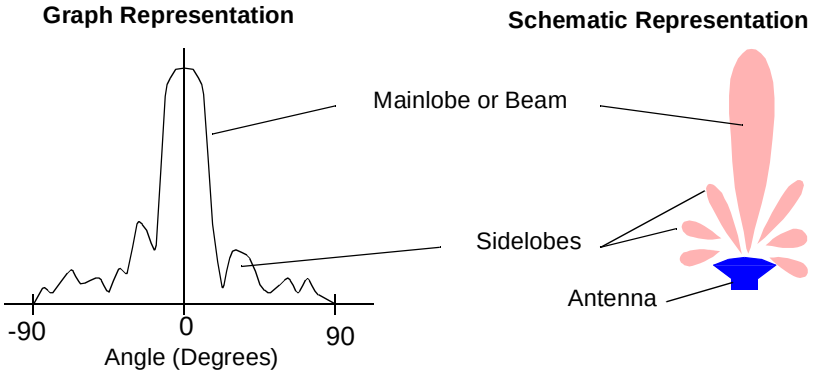

FIGURE 2. Graphic and schematic representations of an antenna-radiation pattern. The graph on the left shows the gain of the antenna at each angle from the front. On the right, the length of the shaded areas is proportional to the gain not to the maximum range.

The antenna-radiation pattern is a geometric property of a radar antenna. It describes the sensitivity of an antenna to a signal at a particular incidence angle. This pattern is usually the same for transmission and reception. A directional antenna concentrates most of its sensitivity in one small area in the front. Similarly, it radiates most of its power in that area, which in turn shapes the radar beam. This sensitivity is generally known as gain; it is expressed in decibels, indicating sensitivity with respect to a perfect omnidirectional antenna. *Figure 2* shows two common representations of a typical radar antenna-radiation pattern.

A two-dimensional scanning radar directs the antenna mainlobe to different areas of the scene. The range measurements form a range map representing the radar-reflecting surfaces. The scanning can be mechanical or motion free. Mechanically-scanned radars move the antenna or parts of it to direct the beam. Motion-free scanning radar changes the antenna-radiation pattern electronically to direct the mainlobe. *Figure 3* illustrates scene motion-free scanning.

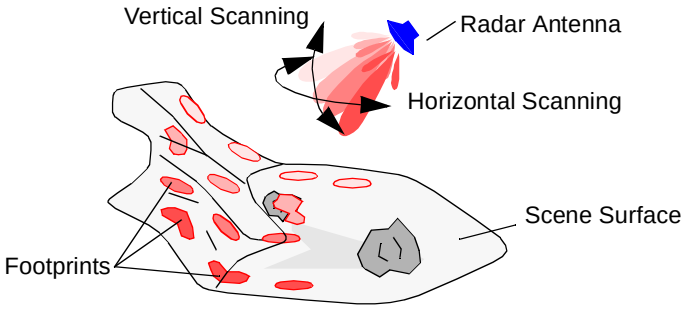

FIGURE 3. Motion-free scanning-radar representation. The sensor directs the mainlobe to vary the vertical and horizontal angles without moving parts.

Angular resolution is the result of low beam divergence (i.e., a narrow beam). The beamwidth is inversely proportional to antenna aperture for a given frequency. For commercial applications, 77 GHz is a common millimeter-wave radar frequency. A 1° beam is achieved with an antenna aperture of 224 mm at that frequency.[1] This applies to both axes in the case of a symmetrical beam defining minimum width and height for the antenna. Achieving a narrower beam requires an impractical antenna size. Therefore, the angular resolution for point targets is limited. Two close targets side by side look like a single one, as illustrated in *Figure 4*.

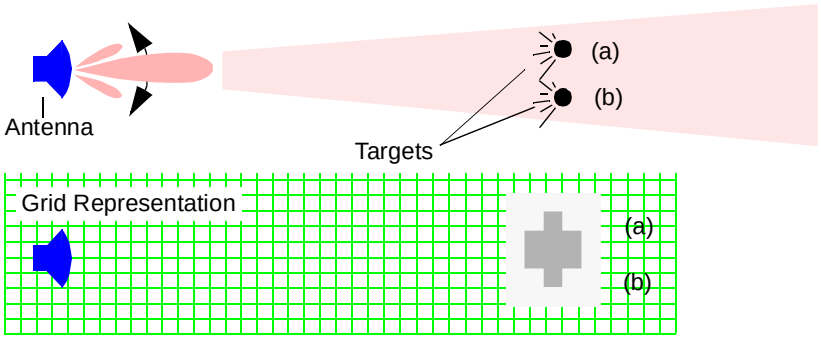

FIGURE 4. Resolution of two targets is possible when the beam is narrower than the gap between two targets. This figure illustrates how scanning with a wide beam will display only one wide target.

Sidelobe false targets are characteristic of radar sensing. Medium-gain areas at angles off the mainlobe introduce false targets: a strong target at a sidelobe area would appear as a target in the mainlobe. No angular discrimination is possible for single-antenna orientation and position. *Figure 5* shows the range-return vector with two signals. Signal (b) corresponds to a target in front of the antenna; signal (a) corresponds to a strong target off the mainlobe. It is impossible to determine which is a sidelobe target from a single reading. Sidelobe false targets can be identified and rejected from a vehicle-mounted

1. Additional information appears in Appendix A.

sensor because they will not appear at other scanning angles or sensor locations. Sidelobes are so relevant to radar sensing that most antenna specification include sidelobe-attenuation information.

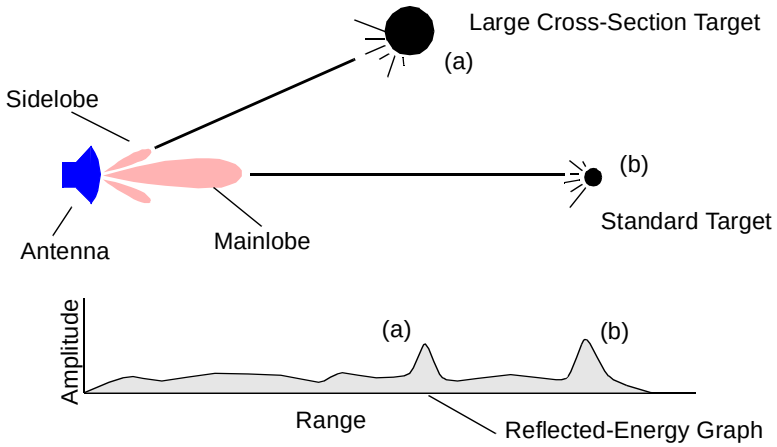

FIGURE 5. A representation of sidelobe false targets. Despite the sidelobe lower gain, a strong target (a) off the mainlobe appears with a signal strength comparable to a smaller target (b) in front of the antenna. Both targets appear in the reflected-energy vector suggesting a wrong location and cross section of target (a).

Reflection targets exist in radar as well as in sonar and laser perception. For each type of radiation, surface types exist that are specular and that reflect transmitted energy away from surfaces. This inhibits perception of the reflecting surface and introduces false targets that backscatter energy back through the inverse reflected path. These false targets appear because they are farther away from the front of the antenna. *Figure 6* shows how a reflecting surface makes target (a) appear in the reflected-energy graph.

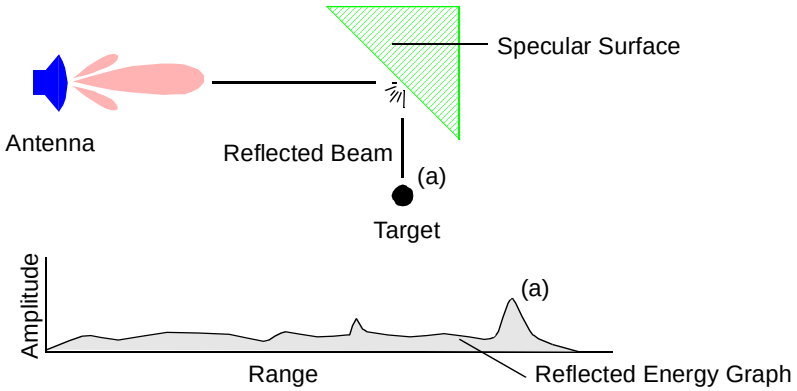

FIGURE 6. Reflected false target: Target (a) is reflected as being in front of the sensor (i.e., farther away).

Adoption of motion-free techniques to steer the beam introduces additional complexities. Traditional antennas provide narrow beams and a high incidence of sidelobe rejection .... properties that remain constant as the antenna is mechanically scanned. Motion-free scanning antennas exhibit varying antenna-radiation pattern, and also poor performance at large scanning angles. The antenna pattern changes with each new beam posi-

tion. The main beam widens, its gain changes and sidelobe attenuation is poorer for high steering angles. The constant variation of these properties complicates processing of the range data. *Figure 7* shows a set of radiation patterns for four scanning angles.

Antenna Radiation Pattern for Four Scanning Angles

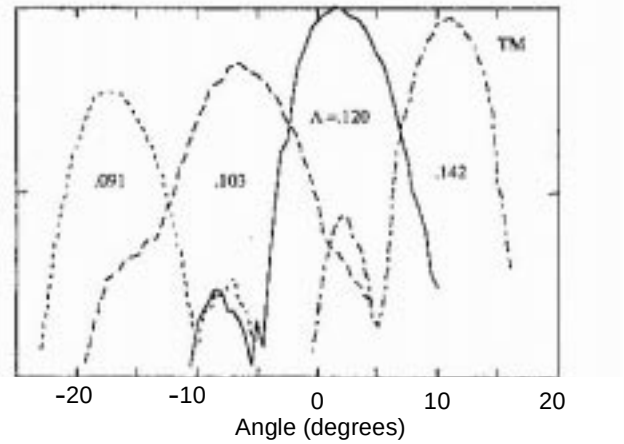

FIGURE 7. An antenna-radiation pattern for a motion-free scanning antenna. Motion-free scanning introduces performance variation. The figure shows radiation patterns for beam angles of -18°, -8°, 3° and 11°. The mainlobe changes its gain, and the sidelobes change attenuation and position.

Antenna-property variation during scanning suggests dynamic processing of the data. Attempts to reject sidelobe false targets will not succeed unless the sensor interpreter considers the changing sidelobes.

Research on the use of radar for position estimation [3] suggests that polarization can help robots distinguish landmarks from clutter. Polarization is the orientation of the electric-field vector as it propagates. Any polarization is a special case of elliptical polarization; elliptical polarization is left-hand or right-hand. Special cases are circular and linear polarization, which can be vertical, horizontal or inclined. Antenna design polarizes the transmitted energy and has more sensitivity to that particular polarization. Beam polarization can change during reflection; the geometry of the scene has direct effect. Polarization can reject unwanted targets, increase detection of others or better characterize a surface based on the polarization effect.

Sidelobes, specular reflections, absorption and large footprint generate ambiguity in radar-data interpretation. High amplitude returns, ideally associated with targets in the direction of the beam and at the indicated direction, might be false targets introduced by sidelobes or specular surfaces. Low amplitude signals, usually associated with empty space, may relate to high absorption or specular surfaces. Polarization could provide improved target discrimination. Radar sensing interpretation should consider these characteristics for enhancing perception models.

2.2 Modeling With Short-Range Radar

Limited precedence exists for applying millimeter-wave radar for navigation and obstacle avoidance [4]. For example, three-dimensional short-range imaging was accomplished at frequencies of 35 GHz and 94 GHz for indoor applications. Processing speed

limited real-time imaging to only two-dimensions. The area of interest was divided in cells that contained a binary value to represent the radar evidence of occupation. The research identified reflections as a shortcoming of indoor radar sensing.

Langer developed a four-beam millimeter-wave radar and processed the radar signal to detect automobiles [5]. The sensor transmitted one wide beam to illuminate the scene. It obtained azimuth resolution with no moving parts through comparison of the returns in four receivers. The processing of the information resulted in estimation of target position (lane), amplitude and a decay parameter. The range resolution is appropriate for automated-highway applications but insufficient for detailed terrain maps.

A millimeter-wave radar-based navigation system detected and matched artificial beacons for localization in a two-dimensional scan [3][6][7]. Researchers suggested that an improved method will eliminate the need for an infrastructure through recognition of features and map building during navigation. Typical operating environments will include structures that can be used as navigation points. The approach uses polarization to maximize discrimination of the beacons from the unwanted signals (clutter).

A complete application of radar for obstacle avoidance was implemented on large mining trucks [8][9]. A MMW radar with four vertically stacked beams scanned an angular range of 64°. The sensor was mounted on the front of the truck and proved adequate to detect persons, obstacles and the sides of dirt roads. Linear polarization at 45° was used to attenuate interference from sensors mounted on vehicles operating in opposite direction. A technique of *aging cells* collected the information of sequential frames. The accumulation reinforced real targets and rejects noise.

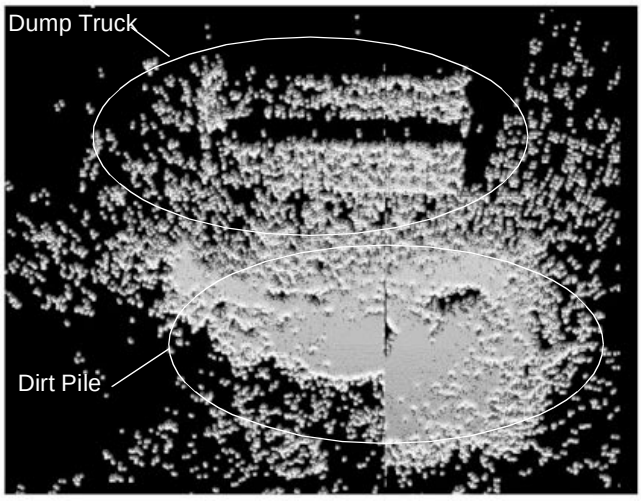

FIGURE 8. An image of a depth map obtained with a 2° radar beam developed at the National Robotics Engineering Consortium. The bed of a dump truck appears in the upper part of the image. The concentration of points in the lower part of the image corresponds to a pile of dirt where the sensor was positioned.

Researchers have succeeded in producing terrain maps from radar perception using pulsed radar with a narrow beam [10]. Dense range maps resulted from a high-sampling rate and a narrow beam of 1°. *Figure 8* illustrates a terrain map of a construction site containing a dump truck and a pile of dirt. Specular and low-reflectivity target perception was obtained through the averaging of multiple samples over the same spot. However, the resulting sensor size was not appropriate for most robotic applications. The

aperture for a 1° beam and wide scanning range resulted in a sensor with a large sweep volume. A second design resulted in a more convenient size at the cost of reduced resolution. The reduced resolution may not be sufficient for robotic operations [11].

2.3 Evidence Grids: a Convenient Representation Tool

The investigation of radar interpretation requires a representation tool that facilitates the study of sensor-scene interaction. Evidence grids are powerful and flexible representation tools that capture the relevant scene aspects for radar-data interpretation. The flexibility of evidence grids facilitates the investigation of and search for appropriate scene parameters such as specularity or surface normal. This research proposal embraces the evidence grid as its representation tool for investigating perception models generated from radar data.

Evidence grids have experienced reformulations and improvements, and different approaches have been presented by several authors. A thorough description of their history and development appears in Reference 17. This reference also includes a comprehensive list of work related to evidence grids and their application. For an excellent description of the use of the stereo-data integration approach appears, see Reference 18. A description follows, introducing the representation of occupancy/emptiness evidence. An extension to represent surfaces is mentioned after.

2.3.1 Representation of Occupancy and Emptiness

An evidence grid represents information about the presence of objects in various positions in space. The approach divides the area or volume of interest into regular cells. Each cell contains a number that represents accumulated evidence of occupancy or emptiness in the space. This number ranges between 0 and 1. A value of 0 designates a certainty of emptiness, and 1 represents certainty of occupancy. A value of 0.5 indicates no evidence of either emptiness or occupancy. All values are usually set to 0.5 before collection of any information or adoption of any assumptions with respect to the environment. *Figure 9* shows a two-dimensional grid generated with sonar sensing on a robot.

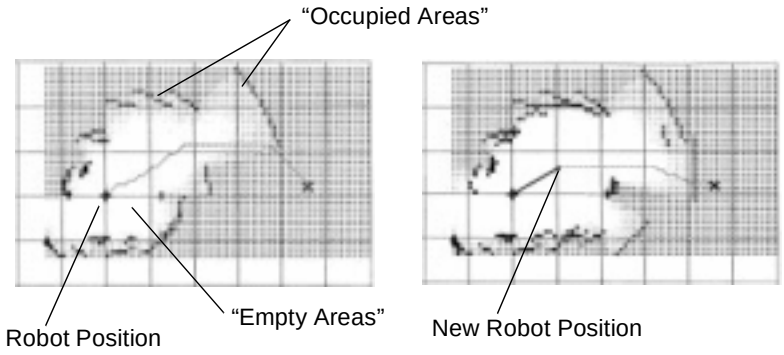

FIGURE 9. Representations of a two-dimensional evidence grid with sonar sensing on a robot. The white areas correspond to evidence of emptiness. The dark areas correspond to evidence of occupancy. Gray areas have no evidence of either occupancy or emptiness. The graph on the left shows the evidence in one robot position. The graph on the right shows the accumulation of sensing in two positions. Illustration extracted from Reference 17.

In the case of radar, a strong return will increase the evidence of occupancy in the corresponding cell. An absence of return indicates evidence of emptiness, and the update occurs accordingly. More parameters associated with each cell can represent additional scene properties. Surface properties are additional features relevant for radar sensing.

Evidence-grids fidelity increases through the accumulation of sensor data. The volume of interest is represented as a regular three-dimensional grid. Each cell of the grid represents accumulated evidence of occupancy or emptiness. A sensor profile represents the sensor data and geometry, and updates the grid cells within the reach of the beam.

The sensor profile represents the sensor geometry and sensitivity of the grid update. Each sensor reading provides new evidence to those cells found within the sensor-beam geometry. The evidence relates to several parameters of the sensor-geometry, propagation and reflection properties. The sensor profile determines the variation of the evidence for each cell of the grid that receives a radar beam. Each element of the sensor profile is a spatial evidence pattern representing the occupancy information implied by a reading, for instance a particular range from a sonar ping or stereoscopic triangulation. The evidence-accumulation operation is an integer-addition operation, representing a Bayesian update, with quantities interpreted as probabilities in log-odds form (i.e., $\log(p/(1-p))$.

Researchers had attempted manual construction of a sensor profile. However, comparisons of the resulting grid against actual scenes facilitated the evaluation of sensor parameters and the pursuit of autonomous learning. Sonar and laser sensor representations have improved because of autonomous learning, allowing for increased resolution and fidelity maps from a comparable number of sensors.

The sensor-profile approach exhibits shortcomings when compared to other scene representations. It is memory- and computation-intensive. Three-dimensional implementation increases the requirements by the number of cells in the new dimension. However, computer developments in memory and processing capacity also improve every year. Therefore, evidence grids will become more and more affordable, along with increased resolution of the cells.

2.3.2 Evidence Grid Extension: Modeling Surfaces

Evidence-grid extensions incorporate additional hypotheses for each cell [12]. Specular reflections, characteristic of sonar sensing, were modeled in a two-dimensional grid. Each cell had additional parameters representing the surface orientation hypothesis. This approach, which applies to radar, expresses the probability of sensing an object as a function of the surface orientation.

3.0 Technical Approach

The proposed research will consider radar-propagation-geometry, reflection and sensor-performance variations to create an interpreter that populates a radar-based evidence grid.

The interpreter will consist of three components: (1) gain adjustment of the range-return vector and application of radar-data heuristics to detect point targets or flat surfaces, (2) incorporation of new information in the grid according to reflection and propagation rules and (3) enhancement of the grid and identification of surfaces. *Figure 10* illustrates a cycle from which perception might proceed from scene sensing to model updating.

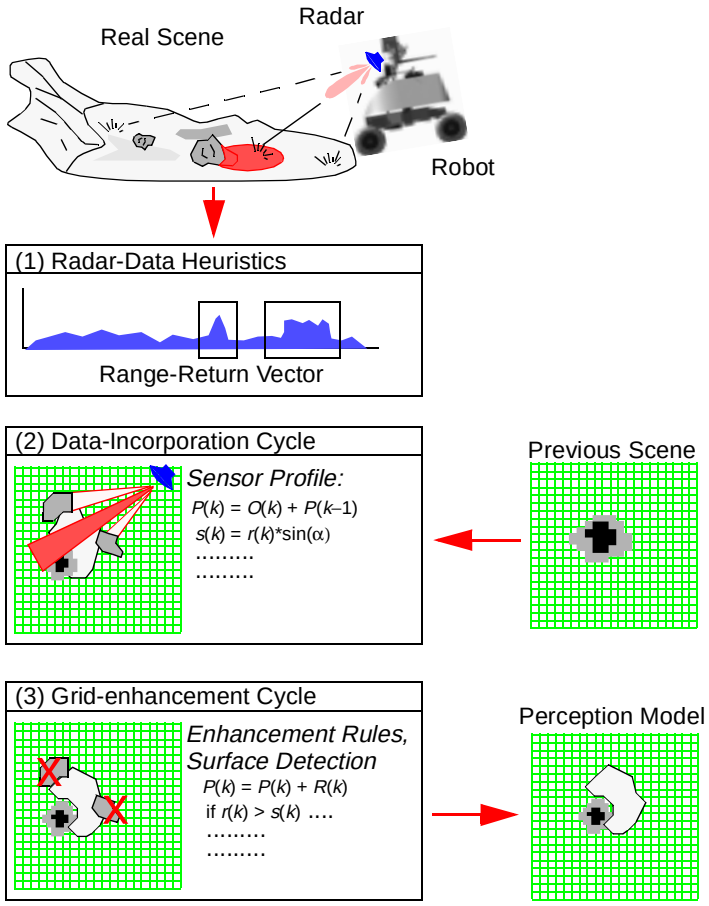

FIGURE 10. Representation of the proposed interpretation cycle. The capturing of a scene through radar sensing goes through (1) the normalization of the range-return vector and application of radar-data heuristics to detect point targets or flat surfaces, (2) incorporation of new information in the grid according to reflection and propagation rules and (3) enhancement of the grid and identification of surfaces.

3.1 Radar-Data Heuristics: Identification of Point Targets and Planes

Recognition of point targets or flat surfaces is possible without any previous scene knowledge. A point target shows a narrow peak in the range-return vector as represented in *Figure 11*. The range precision can be improved through the use of weighted average or curve fitting [13].

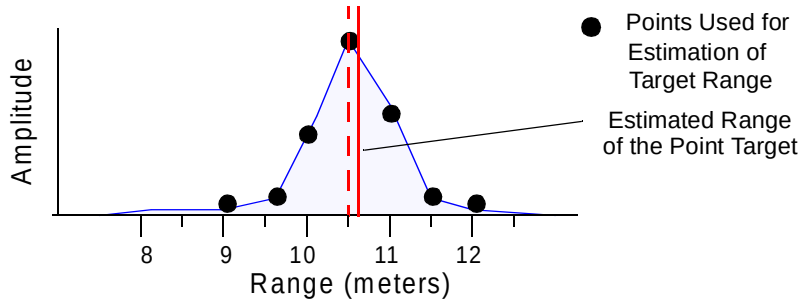

FIGURE 11. A representation of range-precision enhancement. The narrow width of the peak suggests a return from a point target. A precise estimation of the target's range is obtained by weighed average.

Flat surfaces can be identified through interpretation of the range-return vector. A diffuse reflection of the radar beam on a flat surface produces a mesa-like spread. The dimensions of the mesa provide information about the range and orientation of the surface. The beamwidth determines the dimensions of the footprint at the range of the return. The spread is proportional to the sine of the incidence angle. This leads to an estimation of the surface orientation. Figure 12 illustrates a typical return from a flat surface (ground plane) and the associated geometric relation.

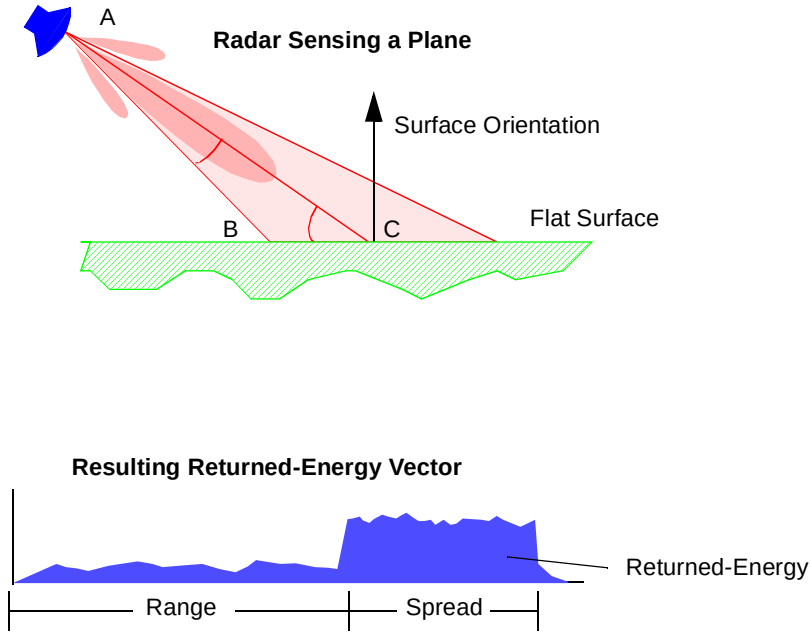

FIGURE 12. A schematic representation of the return from a flat surface. Estimation of surface parameters (orientation) based on the beamwidth and on the range and spread of the return.

Equation 1 and Equation 2 resolve the value of the angle *BCA*. This angle is the relative orientation between the mainlobe and the surface orientation. The letter identifiers are consistent with Figure 12.

$$BC^2 = AB^2 + AC^2 + 2 \cdot \cos(\angle BAC) \quad \textbf{(EQ 1)}$$

$$\angle BCA = \operatorname{asin}\left(\frac{AB}{BC} \cdot \sin \angle BAC\right) \quad \textbf{(EQ 2)}$$

There are two solutions for a two-dimensional grid; the number of solutions is infinite for a three-dimensional problem. The ambiguity can be resolved through storage of the estimated angle for each position. Further measurements will provide enough evidence about a region. A geometric consistency check will resolve the orientation for the area. Eventually, the surface of an object can be estimated using this technique. Surface-orientation description calls for the addition of more parameters to each grid cell; a tailored grid cell will support the interpretation of radar data.

3.2 Radar-Tailored Evidence Grid with Surface Representation

Scene properties affect radar sensing, reflecting the energy to the antenna. This is an effect of the interaction between the beam propagation and the surface of objects. Radar interpretation depends on a scene representation that captures radar-relevant surface properties. Radar-relevant properties include the geometry, roughness and composition of a reflecting surface. The representation of these properties requires additional fields for each cell.

Additionally, the cells store the ambiguity produced by sidelobes and specular reflections; future readings will refer to those values for elimination or retention of uncertain targets. This indefinite-target evidence results from consideration of the antenna-radiation pattern and the reflecting surfaces to predict sidelobes and specular reflection.

An evidence grid tailored for radar perception might have four fields: the standard accumulated evidence of occupancy or emptiness, a measure of the roughness of the surface for specularity evaluation, the orientation or normal of the surface for incidence angle estimation and the accumulated evidence of false sidelobe or reflection targets.

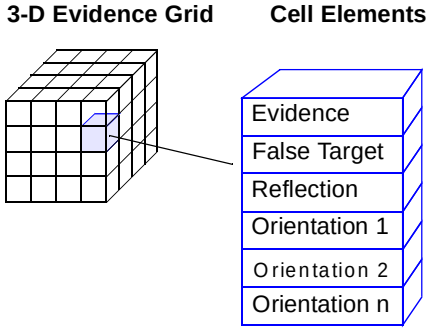

FIGURE 13. Representation of an evidence grid for radar perception. Each cell contains parameters that allow for realistic modeling of the interaction between the radar millimeter waves and the scene.

Cell fields containing emptiness/occupancy evidence and false-target evidence are updated each time a new reading is obtained. Sensor-data incorporation adds new sensor information to the grid according to the sensor profile, as described in Section 3.4.

Surface-property fields are updated periodically based in the actual information of the grid. Surface properties can be recognized once successive readings verify the evidence of occupancy/emptiness. The boundary between strong evidence of emptiness and strong evidence of occupancy defines the surface of objects. Differential operators estimate the surface orientation that is stored in the corresponding field. The grid-enhancing cycles update the surface and orientation estimates.

Failure to detect a known surface or object suggests a specular surface. Specularity is also associated with the incidence angle that causes the detection failure. The roughness estimation is recorded in the specularity field. This field is updated when a reading fails to detect a previously evidenced surface. Also, regular grid-enhancing cycles compare the roughness values of adjacent cells for continuity.

3.3 Sidelobe and Reflection Ambiguity Solving from Sensor Motion

Sensor translation and rotation help to reject false targets caused by sidelobes and reflection. Range measurements taken from different locations will reduce sidelobe uncertainty. Target angular ambiguity will be resolved by the emptiness/occupancy evidence obtained in another sensor location. The same improvement over reflection targets is obtained through consideration of all information in a scene over the sensor motion path. A customized representation of the environment that accounts for reflections and sidelobes will present additional parameters to identify false targets. This value will weigh any additional evidence from another location of the sensor in order to strongly reject false targets, or to increase the evidence of real targets. *Figure 14* illustrates ambiguity resolution with radar data obtained in two locations.

Angular Ambiguity Resolution

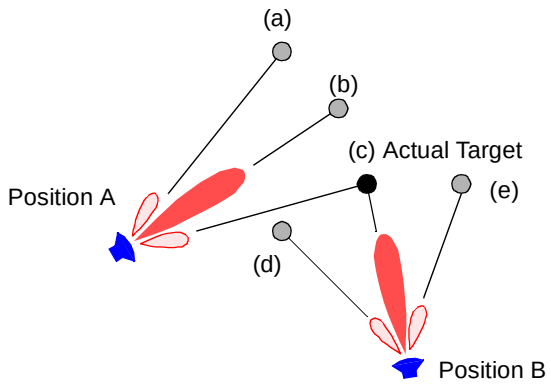

FIGURE 14. Angular ambiguity resolution from sensor in two positions. Targets (a), (b) and (c) could result in the same range measurement with the sensor in position A. Similarly, (c), (d) and (e) are potential targets in position B. combination of evidence from both positions resolves that the actual target is (c).

3.4 Sensor Profile: Multilobe Varying Geometry

The antenna-radiation pattern and antenna-polarization graphs contain mainlobe and sidelobe shape and intensity, as well as the polarization. The antenna-radiation pattern is captured by the radar sensor profile. The sensor-update function refreshes the evidence grid with the new radar data. This function relates to the energy-return vector, the location and orientation of the sensor and the cells of the grid being updated.

3.4.1 Radar - Multilobe Sensor Profile

The antenna-radiation pattern usually includes a mainlobe and sidelobes. This multilobe geometry shapes the *sensor profile*. *Figure 15* shows a scheme of the correspondence between the antenna-radiation pattern and the effective evidence-grid update area for a given sensor location and orientation.

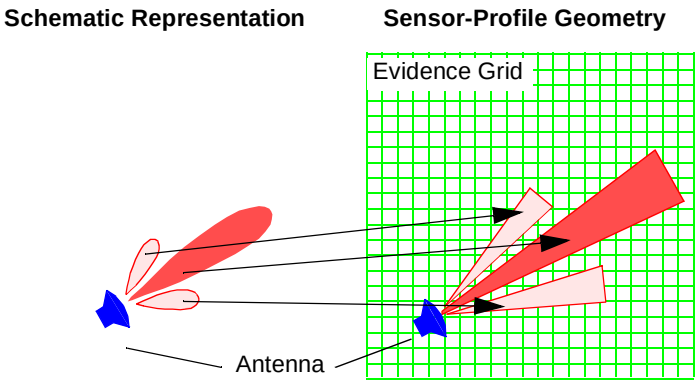

FIGURE 15. A representation of a multilobe sensor-update geometry based on an antenna-radiation pattern. In this case, the antenna-radiation pattern has three relevant lobes: the mainlobe and two sidelobes.

The evidence variation in the mainlobe and in the sidelobes will differ. The sensor profile also updates the values of the false-target probability.

3.4.2 Evidence from Reflected Beams

Specular reflection diverts the direction of the beam as well as the shape and sensing capacity. Evidence grids with surface-angle and surface-reflectivity values allow extension of the sensor profile. The sensor and surface relative position along with orientation result in incidence and reflection angles. *Figure 16* illustrates the effect of a known surface that will reflect the beam. The sensor model adapts its shape to accommodate for the interaction of the beam and the reflecting surface.

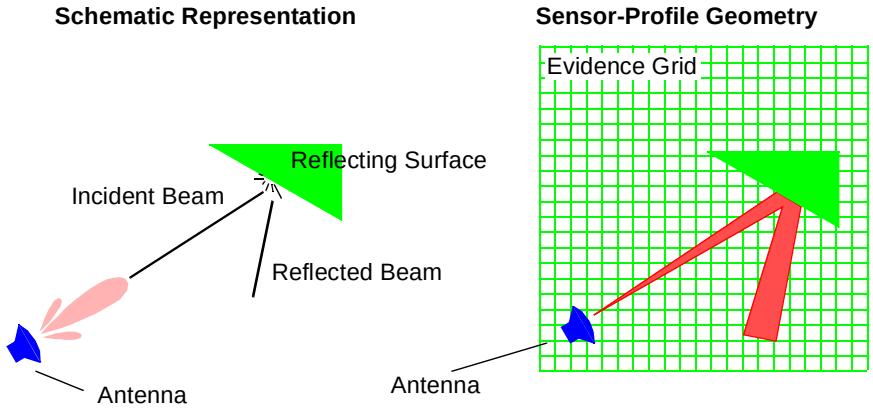

FIGURE 16. A representation of the sensor-geometry update for a specular surface. The update geometry is extended to provide evidence for the mirror symmetric area. The extension accounts for the surface orientation and incidence angle.

3.4.3 Variations in the sensor profile

A varying sensor profile provides compensation for antenna-radiation pattern variations due to scanning. *Figure 17* shows how the sensor model will update cells according to the proper radiation pattern for the current scanning angle. This involves representing variation in both sensitivity and shape. *Figure 17* illustrates the change in the position of the sidelobe and its representation in the sensor-profile geometry.

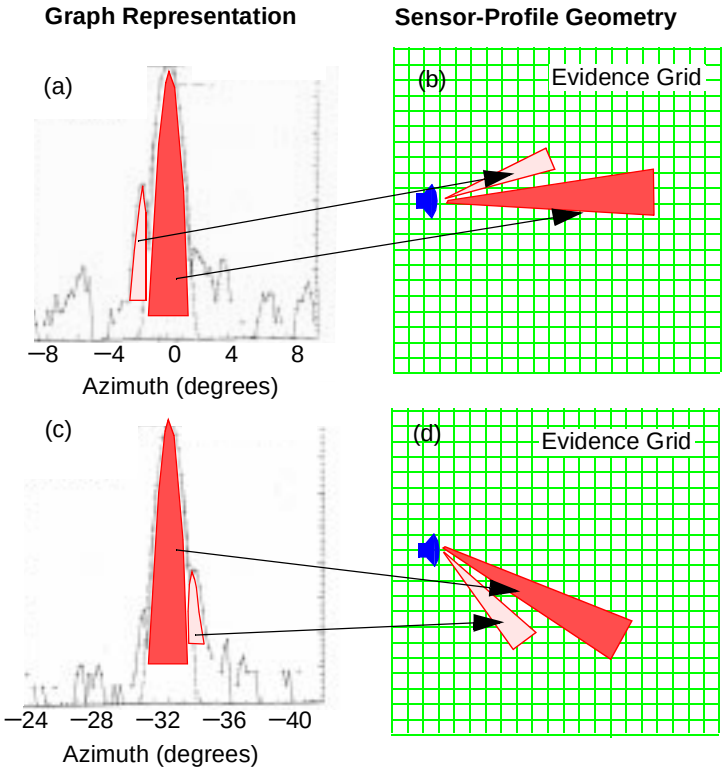

FIGURE 17. A representation of variable sensor geometry. The graph (a) represents the antenna-radiation pattern for a scanning angle of 0°. Note the sidelobe to the left of the mainlobe. Scheme (b) illustrates the sensor geometry for a grid update. Similarly, graph (c) corresponds to the radiation pattern for a scanning angle of -32°. Scheme (d) is the corresponding sensor geometry with a sidelobe to the right of the mainlobe.

4.0 Early Research

During the past year, I studied and experimented with short-range radar perception. Controlled experiments indicated shortcomings of radar such as limited range resolution and a large footprint. Field deployment in a polar environment highlighted the advantages of the proposed sensing modality under compromised-visibility conditions. Research on motion-free antennas uncovered varying antenna-radiation patterns. A two-dimensional implementation of evidence grid indicates that accumulation of radar data obtained from a mobile platform improves scene perception. Research on the availability of radar hardware suggests the practical limits of performance. The results support the proposed thesis: A radar-specific interpretation will enhance a robotic perception model generated from short-range radar.

4.1 Radar Experimental Characterization

The creation of a specific representation of the environment calls for an understanding of the properties of propagation, refraction and reflection of millimeter-radar waves. For that reason, a characterization of the radar in controlled conditions was a necessary first step.

Radar characterization was the first project in support of this research proposal. It identifies strengths and problems of millimeter-wave radar perception. Beamwidth and angular-sampling increments define the angular resolution. The frequency sweep relates to the range bins, defining range accuracy and resolution. Tests on various controlled cases provide insight into shortcomings and possible improvements.

The sensor –a 77-GHz millimeter-wave radar– is showed in Figure 18. Separate antennas transmit and receive radar radiation. The beam shape is 2° in elevation and one degree in azimuth. A moving plate provides horizontal scanning in steps of 1° across 64°. Sequential switching of the beam among four positions provides vertical scanning. A stand with a pitch axis allows aiming at different grazing angles.

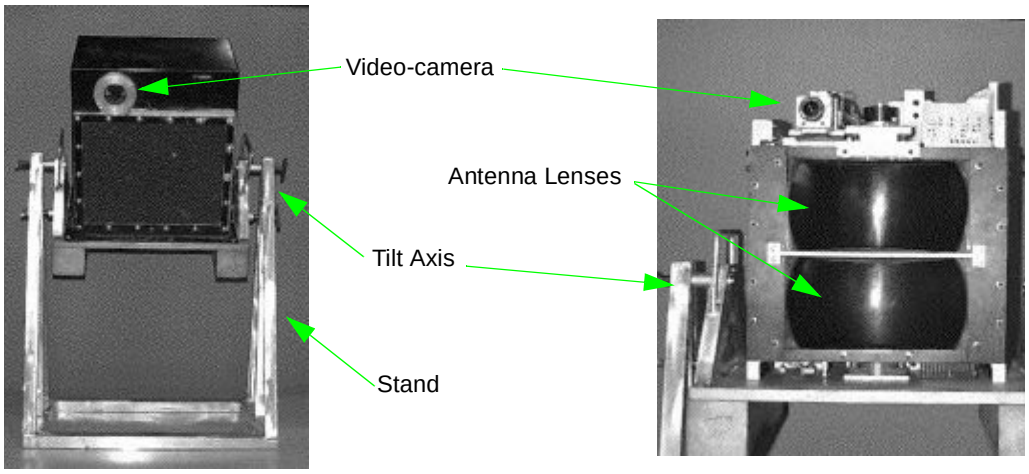

FIGURE 18. Two views of the sensor. The image on the left shows the radar equipment on the stand, with the sensor tilted slightly downward. A video camera allows simultaneous recording of the scene. The image on the right shows the sensor without the protective case. The two black antenna lenses (receive and transmit) shape the 1°-by-2° beam.

4.1.1 Range-Precision Experiment

This experiment evaluates the precision of range measurements. The radar senses a target 10.5-m and 10.6-m away. Although the signal peak remains in the same range bin, small-interval increments of target range are noted by changes in the target-return curve. Figure 19 compares the change for a difference of 0.1 m.

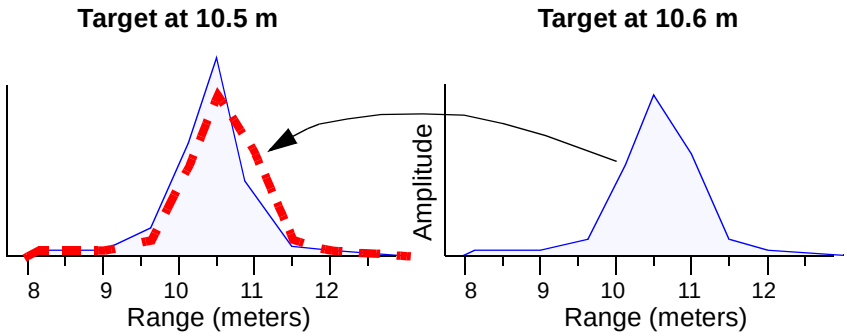

FIGURE 19. Point-target range precision estimation. The graph on the left corresponds to a target 10.5 m from the sensor. The segmented line superimposed shows the shape of the graph to the right; which this time is a target 0.1-m away. Both maximum values are 10.5 m indicating the same range. The slight difference in the graphs suggests that the precision of the sensor can be improved.

4.1.2 Range-Resolution Experiment

The result in Section 4.1.1 indicates that the precision of the range can improve despite the range-bin discretization. This experiment presents the sensor's ability to resolve two targets in which the resolution is lower than the range bin discretization.

The experiment consists of placing two targets on the same direction from the sensor; one remains at 8 m in front of the sensor, the other is moved 4-m to 7.5-m away from the sensor in increments of 0.5 m. When the two targets are at a relative distance of 1.0 m apart, they appear as only one target. Graph (C) in Figure 20 shows two returns merged into one when the distance is 1.0 m.

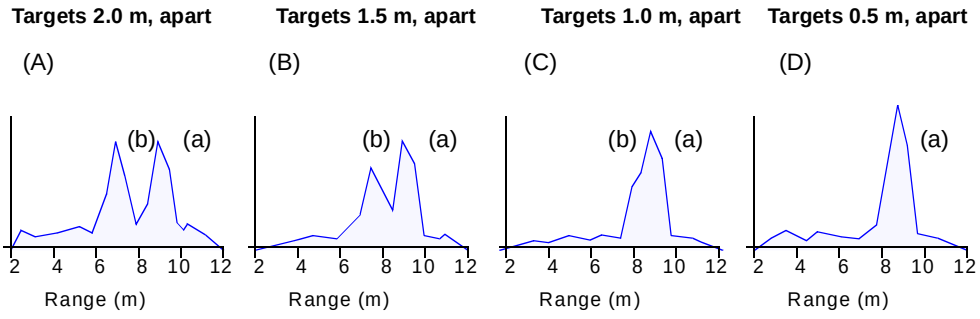

FIGURE 20. A representation of limited range resolution. The figure shows a sequence of scenes with a target (a) at a fixed distance of 9 m from the sensor. Another target (b) appears at an increasing range away (7, 8.5, 9 and 9.5 m) from the sensor. The sensor does not resolve targets closer than 1 m to each other.

4.1.3 Beamwidth-Estimation Experiment

The beamwidth is the width of antenna mainlobe at some specified level. Typically it is the level at which radiated power density is one-half the maximum value on the beam axis. Beamwidth at this level is known as *half-power* or *-3 dB beamwidth.*

A beamwidth-characterization experiment usually uses a fixed transmitter and an antenna on a rotating platform. This experiment moves a reflector across the radar beam and records the intensity for each position, as illustrated in *Figure 21*. Use of identical antennas for transmission and reception results in the half-power threshold appearing as one-quarter of the peak power.

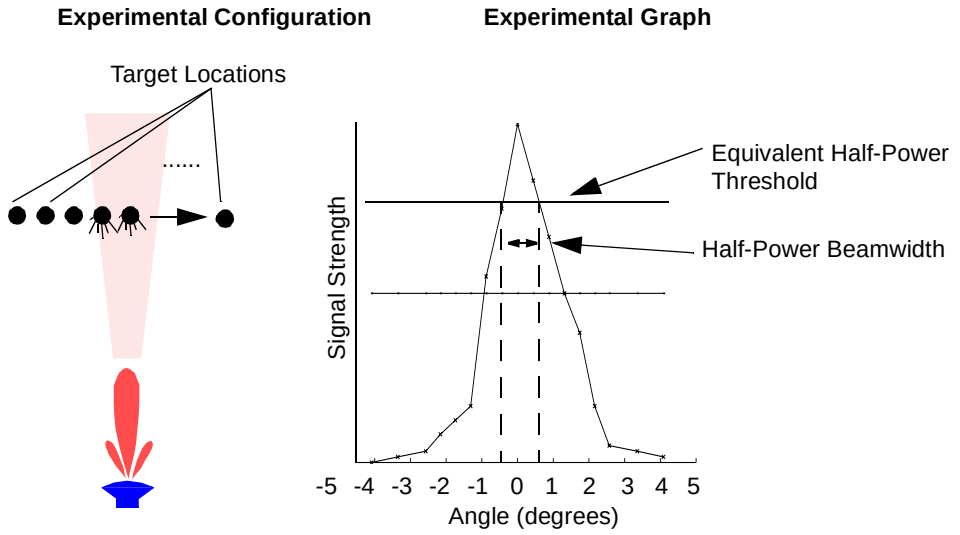

FIGURE 21. A representation of experimental estimation of the beamwidth. A cone reflector is displaced incrementally across the beam to estimate the detection power at different angles from the center of the beam. No sidelobes were detected.

The experimental beamwidth is 1.2°. Sidelobes do not appear in this experiment, probably because of the low angular sampling. Figure 21, on the left, illustrates the experiment configuration. The graph on the right shows the energy return (experimental) and the threshold for estimating the half-power beamwidth.

4.2 Antenna Performance Variation with Scan Angle

The study of a few mechanical and motion-free scanning antennas revealed the varying antenna-radiation pattern associated with the motion-free scanning. Figures 7 and 17 show experimental graphs of motion-free scanning antennas. They indicate mainlobe gain as well as sidelobe gain and position change.

4.3 Evidence Grid Implementation

This section presents two examples of accumulated data with a two-dimensional implementation of evidence grids: a single target scene, and convex and concave obstacle scene. Both incorporate multiple readings into the grid.

4.3.1 Single-Target Scene Modeling

Implementation of a two-dimensional grid incorporated radar readings from different positions. A grid with four readings showed improved precision compared to a single-reading grid. This implementation represents the correct-beam geometry in the sensor profile. See *Figure 22* for an image of the grid. A dark color indicates evidence of emptiness. A light color indicates evidence of occupancy – the target.

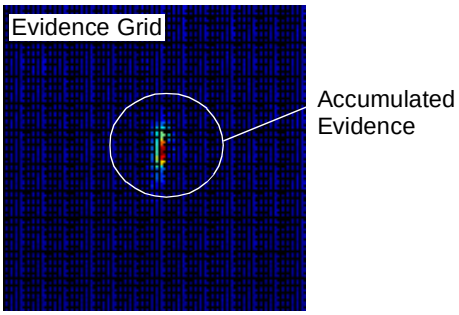

FIGURE 22. Image showing results of single-target radar-sensing on a two dimensional evidence grid. The accumulation of multiple readings showed improved precision over a single-reading image.

4.3.2 Concave and Convex Obstacles Modeling

The same grid implementation served as an experiment of modeling convex and concave obstacles. The image on *Figure 23* illustrates the resulting scene representation. The representation identifies the vertical walls but fails to detect the closer border of the concave obstacle (hole). Similarly, occlusion prevents sensing the back of the convex obstacle (pile).

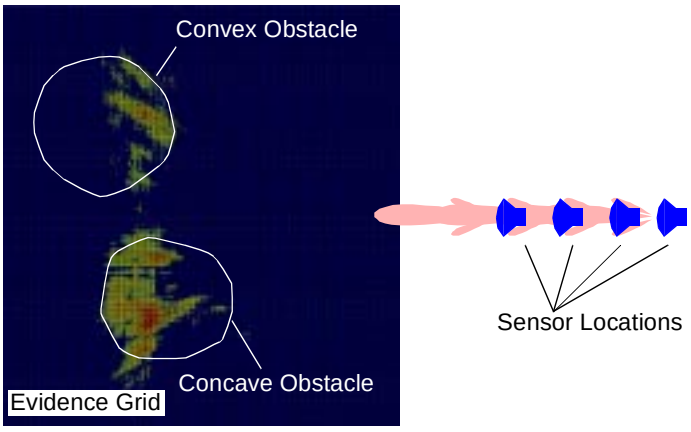

FIGURE 23. An image of obstacle radar sensing on a two-dimensional evidence grid. The resulting representation showed improved precision in comparison to single-reading images. The antennas show the position of the sensor relative to the obstacles.

5.0 Proposed Research Plan and Schedule

5.1 Proposed Research

I will investigate radar sensing to create a new interpretation method to address radar-sensor shortcomings. Radar-data heuristics will provide early feature identification. Evidence grids, suggested by wide-beam sensing developments, will provide a representation tool appropriate for radar-sensing research. A sensor profile will capture radar multilobe sensing, and varying-radiation patterns characteristic of a motion-free scanning antenna. Estimation of surface properties will allow for accurate interpretation of radar data. The interpreter will integrate these techniques, and experimental testing will demonstrate enhancement of the perception models.

5.2 Research Tasks

The research will proceed via 7 tasks, culminating in thesis submission by August 2000.

Interpreter design. The task here is to design an interpreter that accepts a raw radar signal, normalizes it and applies heuristic rules. The interpreter will also incorporate multilobe data into an evidence grid and will recognize surfaces. The result will be a template to serve as the context for component research and as the model for integrating components into a culminating capability of radar modeling. *(June – July 1999)*

Radar data heuristics development. At this stage, I will develop rules for extracting features such as points and planes from radar signals. This task will involve experimentation to calibrate and validate results. *(August – September 1999)*

Radar-sensor profile development. This task will develop a methodology for incorporating the multiple lobes of radar-sensor data into an evidence grid. The development will consider variation of the antenna-radiation pattern and reflection extensions in the sensor profile. The task will result in a dynamic multilobe-sensor profile for radar-data incorporation into the evidence grid. *(October – November 1999)*

Surface-extraction development. I plan to develop a methodology for extracting surface properties from the evidence grid, that are relevant for modeling the specular reflection typical of radar sensing. The outcome will be a component that enhances an environmental representation estimating surface geometry and reflection properties. *(December 1999 – January 2000)*

Integration of interpreter components. This task integrates previous developments – radar-data heuristics, radar-sensor profiles, and surface-extraction components – into a functional interpretation technique that receives radar data and builds a perception model. *(February – March 2000)*

Radar interpreter evaluation. This task will apply experimental data to the interpreter for evaluation of the fidelity increase in the perception model. Experimentation to evaluate components and the integrated interpreter will take place. The result will be a quantitative evaluation of the perception-model enhancement. *(April – May 2000)*

Dissertation composition and presentation. This task will present the results of the proposed research and compose the thesis. The result will be the final document and a presentation for defense of the thesis. *(June – August 2000)*

6.0 Bibliography

[1] M. Skolnik, *Radar Handbook*, 2nd edition (McGraw-Hill, New York, 1989).

[2] D. Barton and S. Leonov, *Radar Technology Encyclopedia* (Artech House Inc., Boston, 1997).

[3] S. Clark and H. Durran-Whyte, “Autonomous Land Vehicle Navigation Using Millimeter Wave Radar,” *Proceedings of the 1998 IEEE International Conference on Robotics and Automation* (May 1998, Leuven, Belgium).

[4] M. Lange and J. Detlefsen, “94 GHz Three-Dimensional Imaging Radar Sensor for Autonomous Vehicles,” *IEEE Transactions on Microwave Theory and Techniques* **39** (5) pp. 819-827.

[5] D. Langer, “Proposal for an Integrated MMW Radar System for Outdoor Navigation,” *Technical Report CMU-RI-TR-96-15* (Robotics Institute, Carnegie Mellon University, Pittsburgh, 1996).

[6] H. Durrant-Whyte, E. Bell and P. Avery, “The Design of a Radar-Based Navigation System for Large Outdoor Vehicles,” *Proceedings of the 1995 IEEE International Conference on Robotics and Automation* (Nagoya, Japan 1995) pp. 764/769.

[7] S. Clark and H. Durran-Whyte, “The Design of a High Performance MMW Radar System for Autonomous Land Vehicle Navigation,” *Proceedings of the International Conference on Field and Service Robotics*, (Zelinsky, eds. Australian Robotic Association Inc Sydney, Australia, 1997) pp 292-299, A

[8] U.S. Patent No. 5,587,929, "System and Method for Tracking Objects Using a Detection System", December 24, 1996. League and Lay of Caterpillar Inc.

[9] U.S Patent No. 5,668,739 "System and Method for Tracking Objects Using a Detection System", September 16, 1997. League and Lay of Caterpillar Inc.

[10] S. Boehmke, J. Bares, E. Mutschler, K. Lay, "A High Speed 3D Radar Scanner for Automation," *Proceedings of the 1998 IEEE International Conference in Robotics and Automation* (Leuven-Belgium, May 1998).

[11] Conversations with Scott Boehmke, National Robotics Engineering Consortium, about the second generation of pulsed MMW radar for terrain mapping, fall 1998, National Robotics Engineering Consortium, Pittsburgh, Pennsylvania.

[12] Ryohei Takada, “Modeling Surface Orientation in 2D Evidence Grids”, *Technical Report 93-026* (Mechanical Technology R&E Center, Nippon Steel Corporation, Chiba, Japan).

[13] "Icebreaker: A Lunar South Pole Exploring Robot," *Technical Report CMU-RI-TR-97-22* (Robotics Institute, Carnegie Mellon University, Pittsburgh, 1997).

[14] A. Johnson, P. Leger, R. Hoffman, M. Hebert and J. Osborn, "3-D Object Modeling and Recognition for Telerobotic Manipulation," *Intelligent Robots and Systems* (1995) pp. 104/110.

[15] R. Zelenka and L. Almsted, "Flight Test of 35GHz MMW Radar Forward Sensor for Collision Avoidance," First World Aviation Congress (1996).

[16] K. O'Neill, "The state of the art of modeling millimeter-wave remote sensing of the environment," *Cold Regions Research & Engineering Laboratory Special Report 96-25* (Cold Regions Research & Engineering Laboratory, 1996).

[17] M. Martin and H. Moravec, "Robot Evidence Grids," *Technical Report CMU-RI-TR-96-06* (Robotics Institute, Carnegie Mellon University, Pittsburgh, 1996).

[18] H. Moravec, "Robot Spatial Perception by Stereoscopic Vision and 3D Evidence Grids," *Technical Report CMU-RI-TR-96-34* (Robotics Institute, Carnegie Mellon University, Pittsburgh, 1996).

[19] V. Manasson, L. Sadovnik, V. Yepishin, "An optically controlled MMW Beam-Steering Antenna Based on a Novel Architecture," *IEEE Transactions on Microwave Theory and Techniques* **45** (8) 1997.

[20] G. Webb, S. Rose, M. Sanchez, J. Osterwalder, "Experiments on an Optically Controlled 2-D Scanning Antenna", *Proceedings of the 1998 Antenna Applications Symposium, Monticello-Illinois.*

[21] N. Vandapel, S.J. Moorehead, W. Whittaker, R. Chatila and R. Murrieta-Cid, "Preliminary Results on the Use of Stereo, Color Cameras and Laser Sensors in Antarctica," *Proceedings of the 1999 International Symposium on Experimental Robotics* (Sidney, Australia, 1999).

[22] I.S. Kweon, R. Hoffman, and E. Krotkov, Experimental Characterization of the Perceptron Laser Rangefinder, *Technical Report CMU-RI-TR-91-01*, (Robotics Institute, Carnegie Mellon University, Pittsburgh, January, 1991).

[23] S. Singh and J. West, Cyclone: A Laser Scanner for Mobile Robot Navigation, *Technical Report CMU-RI-TR-91-18*, (Robotics Institute, Carnegie Mellon University, Pittsburgh, September, 1991).

Appendix A Radar Properties

A.1 Beamwidth, Frequency and Antenna Aperture

Beamwidth is the width of the antenna mainlobe at some specified level of power. Typically, it is the level at which radiated power density is one-half the maximum value of the beam axis. The aperture (i.e., size) of an antenna is related to the frequency and the beamwidth. To achieve a desired beamwidth, a radar's aperture is governed by the following equation:

$$D = \frac{\lambda}{\Theta} \quad \textbf{(EQ 3)}$$

where D is the aperture size, λ is the wavelength of the emitted beam, and θ is the desired beam width. Table 1 lists the required antenna aperture (in millimeters) to achieve the given beam widths (in degrees) for 77 GHz.

TABLE 1. Relation between antenna aperture and beam width

Beam Width at 77 GHz	**5°**	**2°**	**1°**
Aperture Size (mm)	44	112	224

A.2 Range Precision and Resolution

Transceiver performance and the signal processor determine radar-range resolution.[1] In pulsed transceivers, high resolution is obtained with very short pulses and fast counters to measure the return. In FMCW transceivers, range resolution depends mainly on linear frequency sweep range. Equation 4 defines the minimum range bin as a function of the speed of light and the frequency sweep. A frequency sweep of 600 MHz results in range bins of 0.25 meters.

$$\Delta R = \frac{c}{2 \cdot f_s} \quad \textbf{(EQ 4)}$$

A.3 Specular Surfaces

Surface relief determines the reflection of radar energy. Diffuse reflection provides the backscatter necessary for detection. Diffuse reflection depends on the incidence angle (α), wavelength (λ) and the surface corrugation (h). The Rayleigh criterion suggests diffuse reflection according to the following equation:

$$h > \frac{\lambda}{8 \cos \alpha} \quad \textbf{(EQ 5)}$$

Similarly, specular reflection is obtained when the following inequality is satisfied:

$$h > \frac{\lambda}{4 \cos \alpha} \quad \textbf{(EQ 6)}$$

1. Resolution: the ability to distinguish between signals from two adjacent sources.

A.4 Near/Far Field

Most discussion and usage of radar assume wave propagation in the far field. The far field is defined in several ways. It generally refers to a distance far enough (usually more than a wavelength away) from the antenna to be approximated as a plane wave. Exactly how far away the transition from near field to far field occurs is a function of the wavelength, the geometry and size of the antenna. In the immediate vicinity of the antenna called the “near field”, the behavior of wave propagation is different than it is in the “far field”. Some radars filter the data and remove the near-field effects. The far field is dominated by homogeneous waves, and the near field is dominated by inhomogeneous (or evanescent) waves.

Although a radar beam will appear as a thin cone, the shape is not a true representation of the radar beam. This is true for two reasons: (1) the sidelobes and edges of the "beam" are really the half-power points that exist on the mainlobe with most aperture distributions, and (2) the beam doesn’t disperse in the fan shape until it has traveled into the far field, which occurs several aperture diameters from the radar unit. The far-field point is given by the equation:

$$R_F = \frac{2D^2}{\lambda} \qquad \textbf{(EQ 7)}$$

where D is the aperture size and λ is the wavelength.

Appendix B Extreme Weather Validation of Radar Sensing

Experiments evaluate the performance of the sensor operating in the following cases: sensing through severe polar weather, perception of surfaces at high grazing angles and the perception of convex and concave obstacles having the texture of snow.

The atmospheric-absorption experiment measures the effect of flying snow on the sensor. Flying snow absorbs and disperses radar energy, impeding the perception of background features. Two similar scenes are scanned, one with clear air and one with flying snow. A comparison of the results indicates the performance degradation. This experiment also measures the energy returned by the flying particles.

Preliminary results show that blowing snow slightly increases the noise of the perceived scene when compared to similar tests under clear-sky conditions. This compares favorably to the lower performance of laser and stereo under like conditions [21].

The backscatter experiment explores the energy reflected back at different grazing angles on blue ice, fresh snow and packed snow. Blue ice presents a highly specular surface with some undulations carved by the wind. Fresh snow presents soft and rounded profiles. Packed snow contains a combination of flat patches and sharp details. Data are acquired with the radar aiming at fairly flat areas with depression angles between 0° and 14° in increments of 2°. Preliminary results show that all polar surfaces produce diffuse reflection, thus enabling sensing.

The obstacle-detection test simulated the scanning ahead from a vehicle moving towards a concave and convex obstacle, a hole 40-cm deep and a pile of snow of similar height at the side). Deployment and scanning of the scene were performed at regular increments of 25 cm directly approaching the obstacles from a maximum of 9.2 m to a minimum 3.6 m of horizontal distance. Figure 24 shows the sensor in front of the obstacles.

FIGURE 24. Radar deployed in polar terrain. The sensor is aimed at the snow surface for detection of convex and concave obstacles. The figure shows the radar on its pedestal, and the convex and concave obstacles in front of it.